Analytical Approach for Load-carrying Capacity Evaluation of Tibetan Timber Beam-column Joint

Shujie Qin[a], Na Yang[b]*, Xinqun Zhu[c], and Zhijia Wang[a]

[a]*School of Civil Engineering and Architecture, Hainan University, Haikou, China;* [b]*School of Civil Engineering, Beijing Jiaotong University, Beijing, China;* [c]*School of Civil and Environmental Engineering, University of Technology Sydney, Sydney, Australia*

*corresponding author: Na Yang, e-mail: nyang@bjtu.edu.cn

Analytical Approach for Load-carrying Capacity Evaluation of Tibetan Timber Beam-column Joint

Abstract: Queti is an important component of Tibetan timber beam-column joint to transfer compression, shear and bending moment from one structural component to another. The inclination of Queti is a common type of damage in Tibetan heritage buildings and it significantly reduces the load-carrying capacity and safety of the joint under vertical load. In this paper, an analytical model of the joint with Queti-inclination is proposed to predict the yield and ultimate loads of the joint and the corresponding failure modes. Laboratory tests have been conducted on typical Tibetan beam-column joints to verify the proposed model. A parametric study is also conducted on the effects of material property, Queti width and height, as well as the dowel height on the load-carrying capacity of the joint. Results obtained show that a weaker material property will significantly reduce the capacity of the joint. An increase of Queti width and dowel height have an ameliorative effect on the yield and ultimate loads, while the Queti height has the opposite effect.

Keywords: Tibetan timber beam-column joint; Queti-inclination; analytical model; failure mode; load-carrying capacity

Introduction

Tibetan heritage timber buildings in China have high historical, cultural and artistic values. Typical buildings, such as the Potala Palace, Jokhang Temple and Norbulingka Summer Palace, have been on the World Heritage List since 1994. These buildings were subject to a variety of environmental loads with different extents of damage in the last few centuries (Jiang 1994). The different components of these timber structures are connected by joints which are usually the weakest components in the structures (SWRACW 1986). Tibetan beam-column joint (BCJ) has a unique transitional part called the “Queti”, which transfers the compression, shear and bending moment from one structural member to another. Many Queti exhibited the phenomenon of Queti-inclination (Li et al. 2013) which may seriously affect the stability of the timber structure. It is urgent and important to develop a reliable and efficient approach to assess the effect of Queti-inclination on the load-carrying capacity of Tibetan BCJs.

The study on Tibetan building is rare due to its complexity until the last decades. The field survey by Jiang (1994) reported the structural state of the Potala Palace with descriptions on the local damages, their extents and characteristics. Li et al. (2013) summarized the common types of structural damage in Tibetan heritage buildings with discussions on how they were formed from internal and external actions. Yang et al. (2012) studied experimentally the mechanical properties of Tibetan Populus cathayana in the laboratory, with the aim of the evolution of changes in the physical properties between the old and new timber materials. Qin and Yang (2018) proposed a time-dependent model on the strength degradation of timber in the Tibetan heritage buildings with consideration of factors including the material decay, termite attack, temperature and moisture as well as duration of loading.

The structural performances of Tibetan BCJs have been studied only recently. Yang and Qin (2018) explored the effect of different Queti-inclination angles on the structural performances of typical Tibetan timber BCJs in terms of the stiffness, yield load, ultimate load, load-transferring mechanism and failure modes. Five full-scale joint specimens under vertical load were laboratory tested. The Queti-inclination was noted to have a noticeable weakening effect on the load-carrying capacity of the joints. Yan (2011) conducted a series of tests on the rotational behavior of Tibetan BCJs with the comparison of experimental and numerical results. Zhu (2016) experimentally investigated the seismic performances of typical Tibetan timber BCJs under lateral cyclic loading. The stiffness degradation, hysteretic curve, energy-dissipation and failure modes of the joint were studied. Lyu et al. (2017) put forward a temperature-based response sensitivity strategy to identify the connection stiffness of Tibetan BCJs with the Queti modeled as three linear springs.

Tibetan heritage timber buildings are somewhat different from the traditional Han-style buildings. Both Han-style BCJ and Tibetan BCJ use tenon-mortise connection construction. For the Han-style BCJ, the beam and column are directly connected by tenon of beam and

mortise of column. For the Tibetan BCJ, the beams are connected each other by tenon-mortise joint, and the beam and column are connected by Queti. The traditional Chinese Han-style timber joint has also been extensively studied. Existing researches are reviewed because they serve as good references for the study of the BCJs. The structural performances of traditional Han-style timber joints were studied, which includes those on the Dou-Gong brackets (Cao et al. 2021; Chen et al. 2014; Xie et al. 2020), tenon-mortise joints (Chen et al. 2016b; Chun et al. 2020; Li et al. 2020) and column footing joints (He et al. 2017; Wang et al. 2018). The load-displacement (or moment-rotation) relationship, stiffness, load-carrying capacity, deformation mechanism and failure characteristics of the different joints have been analyzed with laboratory models. Others have developed analytical models basing on the elastic-plastic theory to predict the structural performances of typical tenon-mortise joints (Chen et al. 2016; Xie et al. 2014; Pan et al. 2015; Chang and Hsu 2007; Ogawa et al. 2015). Chen et al. (2016a) published a simplified model, with the bending deformation of the tenon neglected, to predict the initial rotational stiffness, yield load, peak load and failure load of the joint. Xie et al. (2014) and Pan et al. (2015) proposed the moment-rotation relation for the joints with dovetail and straight tenon-mortise connections. Theoretical models on traditional butted Nuki joints in Japan and Korea were also developed and validated by scaled and full-sized model tests (Chang and Hsu 2007; Ogawa et al. 2015). Queti-inclination is a typical type of damage in Tibetan heritage buildings (Li et al. 2013). Limited research (Yang and Qin 2018; Qin and Yang 2017; Yan and Yang 2012) has been done to evaluate its effect on the load-carrying capacity of the joints.

This paper studies the evolution of failure mode of the joint with different Queti-inclination angles with the aim to develop an effective analytical approach for the safety evaluation and preservation of Tibetan cultural heritage structures. An analytical model of Tibetan BCJ with Queti-inclination is proposed to predict the load-carrying capacity of the joint with corresponding failure mode. Comparison of the calculated and experimental results is

conducted to validate the feasibility and effectiveness of the proposed model. The influences of mechanical property of timber, Queti width and height, as well as the dowel height on the load-carrying capacity of the joint are also investigated.

Typical Beam-column Joints in Tibetan Buildings

A typical Tibetan structure comprises a combination of conventional framework and supporting system including columns and masonry walls, as shown in Figure 1a. Each room in a Tibetan structure is an independent structural unit with full height walls from floor to ceiling. The enclosed space in the room is spanned with a timber frame system with columns placed directly on stone bases on the floor, and the ends of beams are inserted into the walls. There will be several framed bents in a large room. Figure 1b shows the layout of such a typical Tibetan structural floor system with the "flat roof" feature. The floor slab consists of logs and half round trunks, serving as rafters, placed directly on the top of the beams or walls with diameters varying between 120mm and 180mm. Zhanguns, made of thin timber sticks or planks with diameters varying between 60mm and 80mm, are overlaid on the rafters in perpendicular direction as a constituent layer of Tibetan floor. Cobbles, gravel and agatu (a kind of local soil mixture widely used in Tibetan floor construction) are mixed and placed on the zhanguns. Figure 1c shows the composition of a typical Tibetan beam-column joint, which is composed of a column, a Dianmu, a Gongmu and two beams. The two beams are interconnected by a tenon joint, and the other components are connected by dowels at their contact interfaces. A combination of Dianmu and Gongmu is called a Queti, and it is a special transitional part connecting the beam and column in the Tibetan BCJs. More detail on the traditional Tibetan structural configuration is referred to Ngawang (2007).

A typical Tibetan joint has good in-plane structural performances with bending of Gongmu and the beams. The out-of-plane stability under load, however, is much weaker due to the large height between the head of column and the top of beam, and there is no constraint on

the out-of-plane deformation except at the beam ends and floor level. Queti-inclination, a relative out-of-plane rigid body deformation of the Queti as shown in Figure 2, is often noted during the regular inspection and maintenance of Tibetan heritage timber structures. This inclination is not only due to the out-of-plane deformation from external lateral forces accumulated over the lifetime of the building, but also to the errors in the initial fabrication and assembly, and material defects such as crack, knots and fiber deviation, as well as the long-term effect of eccentricity of the upper load.

Proposed Analytical Model of the Joint

The longitudinal, transverse and height directions of Tibetan BCJ are defined as *x*-, *y*- and *z*-axes respectively, as shown in Figure 1c. The analytical model of the BCJ will be developed in the following sections with the following assumptions:

(1) The vertical load from the floor slab acting on top of the beam follows a uniform distribution.

(2) Vertical forces at the interfaces between beam, Gongmu, Dianmu and column are uniformly distributed along the *x*-axis direction, and they are linearly distributed along the *y*-axis direction.

(3) The influence of bending moment of the components about the *y*-axis direction is neglected.

(4) The constituent materials behave elastically before the joint fails.

(5) The dowel has a rectangular cross-section with the horizontal stress from the mortise uniformly distributed along its height (*z*-axis direction) and width (*x*-axis direction) directions. The dowels are assumed closely matching the mortise without gap.

(6) The column foot is assumed as a hinged joint. (The horizontal force on column due to Queti-inclination under vertical load is generally smaller than the static frictional resistance between column foot and stone base and it will not cause the slippage of

column foot. The column is supported directly on the stone base without any dowel or gluing connection, and the rotational stiffness of column foot is relatively small. The compression deformation and contact area between column foot and stone base are changing when the column is under horizontal load, leading a nonlinearly varying rotational stiffness of column foot. Considering the above problems, it is reasonable and conservative to simplify the column foot as a hinged joint for evaluation of the load-carrying capacity of Tibetan BCJ.)

Assumptions particular to the development of the study will be given along with the discussions.

Load Transmission

The vertical load on the Tibetan BCJ mainly comes from the uniformly distributed load of the upper floor slab and the concentrated load from the upper column foot, as shown in Figure 1a.

The beam on the right-hand-side of the joint as shown in Figure 3 is analyzed. The proportions of load from the uniform load transferred to the Gongmu and wall via the beams are studied. q denotes the uniform line load on the beam from the upper floor slab. q_g and q_w denote the supporting reactions from Gongmu and wall, respectively. q_g can be obtained from force equilibrium as

$$q_g = \frac{2L_b(L_b - L_w)}{L_{g,top}(2L_b - 0.5L_{g,top} - L_w)}q \tag{1}$$

where L_b is the length of the beam; $L_{g,top}$ is the length of Gongmu top surface; L_w is the length of the support on the wall. The load transferred to Gongmu is then calculated as

$$F_{UL,g} = L_{g,top}q_g = \frac{2L_b(L_b - L_w)}{(2L_b - 0.5L_{g,top} - L_w)}q = \frac{(L_b - L_w)}{(2L_b - 0.5L_{g,top} - L_w)}F_{UL} = \eta_g F_{UL} \tag{2}$$

where $F_{UL} = 2L_b q$ is the force from the uniform load on top of two beams. The proportion of load transferred to Gongmu from the uniform load via the beams is

$$\eta_g = \frac{(L_b - L_w)}{(2L_b - 0.5L_{g,top} - L_w)} \tag{3}$$

The load on Gongmu will eventually pass down to the Dianmu and column, which is the true load carried by the BCJ. Another portion of load, $F_{UL,w} = (1 - \eta_g)\, F_{UL}$, is supported by the walls.

The connection between the beams is noted to be a tenon joint and it is effective to transfer the concentrated load from the upper column foot to the Gongmu, while the walls do not share this part of load (Yan and Yang 2012).

The above analysis shows that part of the uniform load on top of beams is carried by the walls, while the rest is transferred to Gongmu and then successively to the Dianmu and column. The concentrated load is fully transmitted to the column without sharing. Therefore, the total vertical load truly carried by the Tibetan BCJ is calculated as

$$F_{tot} = \eta_g F_{UL} + F_{CL} = F_{UL,g} + F_{CL} \tag{4}$$

The BCJ will reach the yield or ultimate limit states with increasing F_{tot}.

Failure Modes

Figure 1c shows that the Dianmu is the most critical and weakest component with the smallest effective compression area in the Tibetan BCJ, which has been confirmed in experimental observation (Yang and Qin 2018) and finite-element modelling study (Yan and Yang 2012). The stress and deformation of the Dianmu are greatly influenced by the Queti-inclination affecting the failure mode and load-carrying capacity of the joint. The evolution of failure mode with Queti-inclination angle θ is studied with the following classification:

(1) Condition 1: Queti is upright (θ =0°). All the components are in uniform compression under vertical load, as shown in Figure 4a. When the compressive strength of timber perpendicular to grain of Dianmu is reached, failure of the joint occurs (material failure).

(2) Condition 2: the angle of Queti-inclination is relatively small ($0° < \theta \leq$critical threshold θ_{cr}). The joint is subject to the additional bending moment and shear force under vertical load due to the out-of-plane deformation induced by Queti-inclination. However, both the shear force and bending moment are insufficient to cause the slippage and rotation of components. The components are in eccentric compression, as shown in Figure 4b. The uneven compressive deformation of Dianmu increases with the vertical load. Similarly, the yielding of Dianmu will result in the failure of the joint with eccentric compressive deformation (material failure).

(3) Condition 3: the angle of Queti-inclination is larger than the critical threshold value ($\theta > \theta_{cr}$). The out-of-plane deformation due to the Queti-inclination introduces a large additional bending moment and horizontal shear force on the Dianmu under the effect of the vertical load. Rotation (Figure 4c) or slippage (Figure 4d) of the contact surface at the Dianmu-column connection or Dianmu-Gongmu connection may occur before the compressive strength of timber perpendicular to grain is reached resulting in failure of the joint (stability failure).

Analytical Model of Load-carrying Capacity of the Joint

Uniform Compression Failure (UC-failure)

The structural performance of the Tibetan BCJ without Queti-inclination will be obtained in this section.

Yield Load. The contact surface between Dianmu and column is at the middle of the joint and it is critically important with the smallest effective compression area. Furthermore, the compressive yield strength perpendicular to grain of the Dianmu is much lower than that parallel to grain of the column. The vertical load that causes yielding of the contact surface between Dianmu and column is therefore defined as the yield load of the joint as

$$F_y = L_{dc1} L_{dc2} C_{\perp L} \quad (5)$$

where L_{dc1} and L_{dc2} are the length (x-axis direction) and width (y-axis direction) of the contact surface between Dianmu and column, respectively; $C_{\perp L}$ is the yield strength of timber perpendicular to grain under partial-area compression (for the length of Dianmu bottom in x-axis direction is larger than that of column head).

Ultimate Load. Figure 5 shows the vertical load-displacement curve of a specimen joint in the laboratory test. The vertical load on the joint behaves linearly with the displacement in the initial loading stage. The load-displacement curve becomes nonlinear with a low and decreasing gradient after F_{tot} reaches $F_y = L_{dc1} L_{dc2} C_{\perp L}$ calculated by Eq. (5). This curve is similar to that for timber perpendicular to grain under compressive loading with no indication of an ultimate load (Chen et al. 2014). The vertical displacement of the joint increases rapidly with a small load increment after material yielding at the contact surface between Dianmu and Gongmu, meaning the imminent failure of the BCJ. Therefore, the ultimate load of the joint can be defined as

$$F_u = L_{dg1} L_{dg2} C_{\perp} \quad (6)$$

where L_{dg1} and L_{dg2} are the length (x-axis direction) and width (y-axis direction) of the contact surface between Dianmu and Gongmu, respectively; $C_{\perp}$ is the yield strength of timber perpendicular to grain under all-area compression (for the length of top surface of Dianmu is smaller than that of Gongmu bottom).

Eccentric Compression Failure (EC-failure)

A simplified analytical model of the Tibetan BCJ with Queti-inclination is shown in Figure 6. Some of the simplifications are described as follows:

(1) The floor slab and the top surface of the beam are packed tightly against each other (Figure 1b). This provides frictional restraint limiting the out-of-plane deformation of the beam. Furthermore, torsional deformation about the longitudinal axis of the beam is

also restricted due to constraints from the walls (Figure 1a). Therefore, when the joint is subject to the vertical load F, the beam will experience the horizontal restraining force along the top surface and restraining torque at one end, i.e. P and M_b. The column foot at the top of the stone base experiences the vertical supporting reaction and lateral frictional force, i.e. F' and P'.

(2) The weakest part of the joint, the Dianmu, is modeled as a connection unit (CU shown in Figure 6) including three spring elements, i.e. K_{Vd}, $K_{\theta d}$ and K_{Hd}, which are the resistances of the Dianmu in vertical compression, out-of-plane bending and lateral deformation, respectively. When the limiting value of a spring element is reached, the joint is considered failed. In other words, the ultimate load-carrying capacity of the joint is determined as the smallest external load that these three spring elements can resist.

When the Queti-inclination angle is not greater than the critical threshold, i.e. $\theta \leq \theta_{cr}$, the joint will fail due to eccentric compression (EC-failure) under the combined action of vertical load and additional bending moment. Yielding of the contact surfaces of Dianmu-column connection and Dianmu-Gongmu connection will lead the joint into the yield and ultimate limit states, respectively.

Yield Load. With reference to the analytical model shown in Figure 6, taking moment at the column foot will give

$$F\left(h_d + h_g\right)\tan\theta = Ph + M_b \tag{7}$$

where $h = h_b + h_g + h_d + h_c$ is the height (z-axis direction) of the whole joint; h_b, h_g, h_d and h_c are the heights of beam, Gongmu, Dianmu and column, respectively.

The out-of-plane bending moment at Dianmu-column connection is

$$M_{dc} = Ph_c = F\left(h_d + h_g\right)\tan\theta - P\left(h_d + h_g + h_b\right) - M_b \tag{8}$$

The case with the BCJ under this additional bending moment M_{dc} is considered. The angle of rigid body rotation of Dianmu is assumed equal to the torsional angle of rotation of the beam cross-section. The ratio of restraining torque to the beam to the resisting bending moment from the Dianmu-column connection is assumed equal to the ratio of the corresponding torsional stiffness of beam to the rotational stiffness of the connection as

$$\frac{M_b}{M_{dc}} = \frac{K_{\theta b}}{K_{\theta dc}} = \kappa \tag{9}$$

where $K_{\theta b}$ and $K_{\theta dc}$ are the restraining torsional stiffness of the beam and rotational stiffness of Dianmu-column connection, respectively. They can be calculated with the following formulas (Liu 2011):

$$K_{\theta b} = \frac{w_b h_b G_{\parallel}(w_b^2 + h_b^2)}{12 l_{be}} \tag{10}$$

$$K_{\theta dc} = \frac{L_{dc1} L_{dc2}^3 E_{\perp}}{12\left(h_d + h_g + h_b\right)} \tag{11}$$

where $G_{\parallel}$ is the shear modulus parallel to grain; $E_{\perp}$ is the modulus of elasticity perpendicular to grain; w_b and l_{be} are the width and torsional length of the beam, respectively.

Combining Eqs. (8) and (9), the restraining torque of the beam can be derived as

$$M_b = P h_c \kappa \tag{12}$$

Putting Eq. (12) into Eq. (7), the horizontal restraining force on the top surface of the beam can be obtained as

$$P = \frac{F\left(h_d + h_g\right)\tan\theta}{h + h_c \kappa} \tag{13}$$

The maximum compressive stress at the Dianmu bottom (the contact surface between Dianmu and column) under the combined action of vertical load and additional bending moment can be given as

$$\sigma_{dc,max} = \frac{F}{A_{dc}} + \frac{M_{dc}}{W_{dc}} = \frac{F}{A_{dc}} + \frac{Ph_c}{W_{dc}} = \frac{F}{L_{dc1}L_{dc2}} \frac{L_{dc2}(h + h_c\kappa) + 6h_c\left(h_d + h_g\right)\tan\theta}{L_{dc2}(h + h_c\kappa)} \quad (14)$$

where A_{dc} and W_{dc} are the effective area and sectional modulus of the contact surface between Dianmu and column.

When $\sigma_{dc,max}$ reaches the yield strength of timber perpendicular to grain, the BCJ will yield and the corresponding yield load can be derived as

$$F_y = L_{dc1}L_{dc2}C_{\perp L} \frac{L_{dc2}(h + h_c\kappa)}{L_{dc2}(h + h_c\kappa) + 6h_c\left(h_d + h_g\right)\tan\theta} = F_{y0}\zeta_y \quad (15)$$

where $F_{y0} = L_{dc1}L_{dc2}C_{\perp L}$ [Eq. (5)] is the yield load of the joint without Queti-inclination, and

$$\zeta_y = \frac{L_{dc2}(h + h_c\kappa)}{L_{dc2}(h + h_c\kappa) + 6h_c\left(h_d + h_g\right)\tan\theta} \quad (16)$$

is the influence coefficient of Queti-inclination on the yield load of the joint.

Ultimate Load. Similar to the derivation process above, the bending moment at Dianmu-Gongmu connection can be obtained as

$$M_{dg} = Fh_d\tan\theta - P(h_c + h_d) \quad (17)$$

When under the combined action of vertical load and additional bending moment, the maximum compressive stress at the contact surface between Dianmu and Gongmu can be obtained as

$$\begin{aligned}\sigma_{dg,max} &= \frac{F}{A_{dg}} + \frac{M_{dg}}{W_{dg}} \\ &= \frac{F}{L_{dg1}L_{dg2}} \frac{L_{dg2}(h + h_c\kappa) + 6h_d(h + h_c\kappa)\tan\theta - 6(h_c + h_d)\left(h_d + h_g\right)\tan\theta}{L_{dg2}(h + h_c\kappa)}\end{aligned} \quad (18)$$

where A_{dg} and W_{dg} are the effective area and sectional modulus of the contact surface between Dianmu and Gongmu.

When $\sigma_{dg,max}$ reaches the yield strength of timber perpendicular to grain, the BCJ is in the EC-failure limit state with the corresponding ultimate load derived as

$$F_u = F_{dge} = L_{dg1}L_{dg2}C_{\perp}\frac{L_{dg2}(h+h_c\kappa)}{L_{dg2}(h+h_c\kappa)+6h_d(h+h_c\kappa)\tan\theta-6(h_c+h_d)\left(h_d+h_g\right)\tan\theta} = F_{u0}\zeta_u \quad (19)$$

where $F_{u0} = L_{dg1}L_{dg2}C_{\perp}$ [Eq. (6)] is the ultimate load of the joint without Queti-inclination.

$$\zeta_{dge} = \frac{L_{dg2}(h+h_c\kappa)}{L_{dg2}(h+h_c\kappa)+6h_d(h+h_c\kappa)\tan\theta-6(h_c+h_d)\left(h_d+h_g\right)\tan\theta} \quad (20)$$

is the influence coefficient of Queti-inclination on the ultimate load of the joint.

Both Eqs. (16) and (20) show that the influence coefficients ζ_y and ζ_{dge} are related not only to the Queti-inclination angle, but also to the size of components of the joint.

Rotational Failure (R-failure)

The additional bending moment induced by the out-of-plane deformation increases with the angle of Queti-inclination under the same vertical load, and the stress distribution on the load-bearing surface of Dianmu (i.e. the contact surfaces of Dianmu-column or Dianmu-Gongmu connections) will exhibit the following stress patterns as:

(1) When the tensile stress induced by the additional bending moment is smaller than the compressive stress induced by the vertical load, i.e. $M_{dc}/W_{dc} < F/A_{dc}$ or $M_{dg}/W_{dg} < F/A_{dg}$, the load-bearing surface of Dianmu is in full compression, as shown in Figure 7a.

(2) When $M_{dc}/W_{dc} = F/A_{dc}$ or $M_{dg}/W_{dg} = F/A_{dg}$, the load-bearing surface of Dianmu is in the critical state of full compression, as shown in Figure 7b.

(3) When $M_{dc}/W_{dc} > F/A_{dc}$ or $M_{dg}/W_{dg} > F/A_{dg}$, the load-bearing surface of Dianmu is in the partial compression state, as shown in Figure 7c.

Since the components of a Tibetan BCJ are overlaid vertically with one on the other without any gluing connection, the non-compression region in Figure 7c of the load-bearing surface carries zero force. The only source that can provide a resisting bending moment within this zone is the dowel between two components as shown in Figure 1c. The dowel is under horizontal forces along its height from the mortise due to relative deformation of the two

components. The horizontal stress is assumed uniformly distributed along the height and width of the dowel as shown in Figure 7d. The maximum resisting moment a dowel can provide may be given as

$$M_a = \frac{1}{16} h_a^2 l_a C_{\perp L} \tag{21}$$

where h_a and l_a are the height and width of the dowel.

When the bending moment resistance generated in the dowel reaches its maximum allowable in Eq. (21), and the maximum stress in the compression zone is lower than the compressive strength of timber perpendicular to grain, the unloaded contact surface between two components will separated with rotation of the Dianmu resulting in failure of the joint.

The ultimate load-carrying capacities of the joint corresponding to the rotational failure (R-failure) at Dianmu-column connection or Dianmu-Gongmu connection will be described below.

Dianmu-column connection. The minimum stress in the contact surface between Dianmu and column is

$$\sigma_{dc,min} = \frac{F}{A_{dc}} - \frac{M_{dc}}{W_{dc}} = \frac{F\left[L_{dc2}(h + h_c\kappa) - 6h_c\left(h_d + h_g\right)\tan\theta\right]}{L_{dc1}L_{dc2}^2(h + h_c\kappa)} \tag{22}$$

By setting $\sigma_{dc,min} = 0$, the Queti-inclination angle $\theta_{dc\prime}$ corresponding to the critical state (Figure 7b) of full compression between Dianmu and column can be obtained as

$$\theta_{dc\prime} = \arctan\left[\frac{L_{dc2}(h + h_c\kappa)}{6h_c\left(h_d + h_g\right)}\right] \tag{23}$$

When $\theta > \theta_{dc\prime}$, the contact surface of Dianmu and column is in the partial compression state as shown in Figure 7c, and the length of the non-compression region is

$$L_{dc2\prime} = \frac{6h_c\left(h_d + h_g\right)\tan\theta - L_{dc2}(h + h_c\kappa)}{12h_c\left(h_d + h_g\right)\tan\theta} \cdot L_{dc2} \tag{24}$$

The bending moment contributed by the non-compression region about the centroid axis of the contact surface is

$$M_{dcr} = \frac{FL_{dc2\prime}(3L_{dc2} - 2L_{dc2\prime})\left[6h_c\left(h_d + h_g\right)\tan\theta - L_{dc2}(h + h_c\kappa)\right]}{12L_{dc2}^2(h + h_c\kappa)} \tag{25}$$

Combining Eqs. (21) and (25) and setting $M_{dcr} = M_a$, the ultimate load corresponding to the R-failure limit state at the Dianmu-column connection can be derived as

$$F_u = F_{dcr} = \frac{3h_a^2 l_a C_{\perp L} L_{dc2}^2(h + h_c\kappa)}{4L_{dc2\prime}(3L_{dc2} - 2L_{dc2\prime})\left[6h_c\left(h_d + h_g\right)\tan\theta - L_{dc2}(h + h_c\kappa)\right]} \tag{26}$$

Combining Eqs. (15) and (26) and setting $F_y = F_{dcr}$, the critical threshold θ_{dc} corresponding to R-failure limit state at the Dianmu-column connection can be obtained.

It is noteworthy that, when θ increases to $\theta_{dc\prime}$, the Dianmu-column connection will be in the partial compression state but the failure mode of the joint is still EC-failure. Only when θ is greater than θ_{dc} that the failure mode will switch to the R-failure as:

(1) When $\theta < \theta_{dc}$, the joint yields due to the EC-failure at Dianmu-column connection.

(2) When $\theta \geq \theta_{dc}$, the joint fails due to the R-failure at Dianmu-column connection.

Dianmu-Gongmu connection. The minimum stress in the contact surface between Dianmu and Gongmu can be written as

$$\sigma_{dg,min} = \frac{F}{A_{dg}} - \frac{M_{dg}}{W_{dg}} = \frac{F\left[L_{dg2}(h + h_c\kappa) + 6(h_c + h_d)\left(h_d + h_g\right)\tan\theta - 6h_d(h + h_c\kappa)\tan\theta\right]}{L_{dg1}L_{dg2}^2(h + h_c\kappa)} \tag{27}$$

By setting $\sigma_{dg,min} = 0$, the Queti-inclination angle $\theta_{dg\prime}$ corresponding to the critical state (Figure 7b) of full compression between the Dianmu and Gongmu can be derived as

$$\theta_{dg\prime} = \arctan\left[\frac{L_{dg2}(h + h_c\kappa)}{6(h_c + h_d)\left(h_d + h_g\right) - 6h_d(h + h_c\kappa)}\right] \tag{28}$$

When $\theta > \theta_{dg\prime}$, the length of non-compression region shown in Figure 7c is

$$L_{dg2'} = \frac{6(h_c + h_d)(h_d + h_g)\tan\theta - 6h_d(h + h_c\kappa)\tan\theta - L_{dg2}(h + h_c\kappa)}{2\left[(h_c + h_d)(h_d + h_g)\tan\theta - 6h_d(h + h_c\kappa)\tan\theta\right]} \cdot L_{dg2} \quad (29)$$

The bending moment contributed by the non-compression region about the centroid axis of the contact surface is

$$M_{dgr} = \frac{FL_{dg2'}(3L_{dg2} - 2L_{dg2'})\left[6(h_c + h_d)(h_d + h_g)\tan\theta - 6h_d(h + h_c\kappa)\tan\theta - L_{dg2}(h + h_c\kappa)\right]}{12L_{dg2}^2(h + h_c\kappa)} \quad (30)$$

Combining Eqs. (21) and (30) and setting $M_{dcr} = 2M_a$ (there are two dowels in the contact surface between Dianmu and Gongmu), the ultimate load corresponding to the R-failure at Dianmu-Gongmu connection can be derived as

$$F_u = F_{dgr} = \frac{3h_a^2 l_a C_{\perp L} L_{dg2}^2 (h + h_c\kappa)}{2L_{dg2'}(3L_{dg2} - 2L_{dg2'})\left[6(h_c + h_d)(h_d + h_g)\tan\theta - 6h_d(h + h_c\kappa)\tan\theta - L_{dg2}(h + h_c\kappa)\right]} \quad (31)$$

Combining Eqs. (19) and (31) and setting $F_{dge} = F_{dgr}$, the critical threshold θ_{dg} corresponding to R-failure at the Dianmu-Gongmu connection can be obtained. The failure mode of the joint changes with the Queti-inclination angle as:

(1) When $\theta < \theta_{dg}$, the joint fails due to EC-failure at Dianmu-Gongmu connection.

(2) When $\theta \geq \theta_{dg}$, the joint fails due to R-failure at Dianmu-Gongmu connection.

Shear Failure (S-failure)

The stress state at the contact surface of Dianmu-column connection of the Tibetan BCJ provides the shear force resistance. It is noted in Figure 6 and Eq. (13) that, the horizontal shear force increases with the angle of Queti-inclination. When the shear force is greater than the sum of the static frictional resistance at the contact surface and the shear resistance of the dowel, the joint fails due to the shear failure (S-failure):

$$P = \frac{F(h_d + h_g)\tan\theta}{h + h_c\kappa} = \mu F + l_a w_a S_\perp > \mu F \quad (32)$$

where μ is the friction coefficient between timber surfaces ranging from 0.4 to 0.6 (Wang et al. 2018); $S_\perp$ is shear strength of timber perpendicular to grain.

Eq. (32) shows that the Queti-inclination angle corresponding to S-failure without considering the shear resistance of the dowel should satisfy the following condition:

$$\theta > \arctan\left[\frac{\mu(h + h_c\kappa)}{(h_d + h_g)}\right] \tag{33}$$

The above model is checked with the set of BCJ specimens shown in Tables 1 and 2. Substituting the information of the test specimen into Eq. (33) and taking μ =0.4, the minimum angle of the Queti-inclination to have S-failure is determined as 85.7°. This angle will increase when the shear resistance of the dowel is considered. Checks on other Tibetan BCJs with different dimensions also give the same conclusion indicating that the BCJ will usually not fail in the S-failure mode.

Change of Load-carrying Capacity with Que-inclination Angle

It may be summarized from the above analysis that the failure mode and load-carrying capacity of the joint under vertical load vary with different angles of Queti-inclination as follows:

(1) $\theta \le \theta_{cr} = \min(\theta_{dc}, \theta_{dg})$

The joint yields when the vertical load reaches F_y in Eq. (15). When the load increases to $F_u = F_{dge}$ in Eq. (19), the joint fails in the UC-failure ($\theta = 0°$) or EC-failure modes.

(2) $\min(\theta_{dc}, \theta_{dg}) < \theta \le \max(\theta_{dc}, \theta_{dg})$

a) When $\theta_{dg} \le \theta_{dc}$, the joint will fail with the R-failure mode at the Dianmu-Gongmu connection as described below. If $F_y \le F_{dgr}$, a vertical load equals to F_y given in Eq. (15) will lead to yielding of the joint at the Dianmu-column connection. When the load increases to $F_u = F_{dgr}$ in Eq. (31), the joint will fail with the R-failure mode at Dianmu-Gongmu connection. If $F_y > F_{dgr}$, a load equals to $F_u = F_{dgr}$ in Eq. (31) will result in the R-failure limit state at the Dianmu-Gongmu connection. This means the joint will lose its stability before yielding of the contact surface between Dianmu and column.

b) When $\theta_{dc} < \theta_{dg}$, and the vertical load reaches $F_u = F_{dcr}$ in Eq. (26), the joint fails with the R-failure mode at the Dianmu-column connection.

(3) When $\theta > \max(\theta_{dc}, \theta_{dg})$ and the vertical load reaches $F_u = \min(F_{dcr}, F_{dgr})$, the joint will fail in the R-failure mode as described below. If $F_{dcr} \leq F_{dgr}$ and the vertical load reaches $F_u = F_{dcr}$ in Eq. (26), the joint fails with the R-failure mode at the Dianmu-column connection. If $F_{dcr} > F_{dgr}$ and the vertical load reaches $F_u = F_{dgr}$ in Eq. (31), the joint fails with the R-failure mode at the Dianmu-Gongmu connection.

The information of the set of BCJ specimens shown in Tables 1 and 2 is substituted into Eqs. (15), (19), (26) and (31) for illustration of the proposed model. Combining Eqs. (19) and (31) and setting $F_{dge} = F_{dgr}$, the angle θ_{dg} is obtained as 32.7°. Combining Eqs. (15) and (26) and setting $F_y = F_{dcr}$, the angle θ_{dc} is obtained as 46.3°. When $\theta \leq 32.7°$, the yield load F_y and ultimate load F_u are calculated by Eqs. (15) and (19), respectively. When $32.7° < \theta \leq 46.3°$, the loads F_y and F_u are calculated by Eqs. (15) and (31), respectively, and F_y should be discarded for $\theta > 33.6°$ since F_y is found to be greater than F_u. When $\theta > 46.3°$, the load F_u is calculated by min[Eq. (26), Eq. (31)]. The variation of yield and ultimate loads with different Queti-inclination angles can be obtained as shown in Figure 8 and discussed below.

(1) When $\theta = 0°$, the joint fails with the UC-failure mode.

(2) When $0° < \theta \leq \theta_{cr} = \min(\theta_{dc}, \theta_{dg}) = \theta_{dg} = 32.7°$, the joint fails with the EC-failure mode. The yield load F_y and ultimate load F_u decrease nonlinearly with the Queti-inclination angle. When $\theta = \theta_{dg} = 32.7°$, the loads F_y and F_u are 41.0% of F_{y0} and 53.3% of F_{u0} respectively, and they are noted less than those of the joint without Queti-inclination.

(3) When $\theta_{dg} < \theta \leq \max(\theta_{dc}, \theta_{dg}) = \theta_{dc} = 46.3°$, the joint fails with the R-failure mode at the Dianmu-Gongmu connection. The ultimate load F_u decreases rapidly with

the Queti-inclination angle. When $\theta > 33.6°$, the joint fails due to R-failure before yielding of the contact surface between Dianmu and column, and there is no yield load any more.

(4) When $\theta_{dc} < \theta \leq 75.1°$, the joint fails in the R-failure mode at the Dianmu-Gongmu connection. When $\theta > 75.1°$, failure occurs at the Dianmu-column connection with the R-failure mode.

Experimental Verification

Tibetan BCJ Laboratory Specimens

Five full-scale specimens of Tibetan BCJs were fabricated with the Queti-inclination angles θ=0.0°, 3.0°, 6.0°, 9.0° and 12.0°, respectively. The angle was created with both Gongmu and Dianmu fabricated with inclined flanks (Figure 9a). The specimens were prepared from Mongolian Scotch pine (*Pinus sylvestris var. mongolica Litv.*) and they were identical with the same dimensions in different components shown in Table 1 but with different Queti-inclination angles. The overall dimensions of the specimens are 190 mm in width, 4400 mm in length and 2110 mm in height. The specimens are duplicates of a Tibetan BCJ in the Potala Palace.

The mechanical properties of timber are greatly influenced by the moisture content (MC) and natural defects such as knots, cracks and fiber deviation. Adjustments to the mechanical properties are needed to consider these effects according to GB/T 1928-2009 (SAC 2009).

The mechanical property X_m of timber with m% of MC can be estimated by the following formula (Long 2005):

$$X_m = X_{12}[1 + \alpha(12 - m)] \tag{34}$$

where X_{12} is the mechanical property with standard 12% MC; α is the adjustment coefficient on the moisture content.

The effect of size and defect on mechanical properties of timber component can be considered with the following reduction coefficient (Long 2005):

$$K_Q = K_{Q1}K_{Q2}K_{Q3}K_{Q4} \tag{35}$$

where K_{Q1}, K_{Q2}, K_{Q3} and K_{Q4} are the reduction coefficients on the size effect, natural defect, drying defect and long-term load, respectively.

The value of MC in the laboratory specimens was 5.4%. The values of α, K_{Q1}, K_{Q2}, K_{Q3} and K_{Q4} can be obtained from the handbook (Long 2005), and they are shown in Table 3. The mechanical properties of timber modified with these coefficients are shown in Table 2.

The test configuration is shown in Figure 9b. The outer beam ends of the specimen were restricted from rotation and out-of-plane movement with two clamps, simulating the conditions in the supporting masonry wall. Two pneumatic jacks and two steel beams were used to distribute the vertical loads simulating the uniform floor loading. The loads were monitored with two 100 kN load cells. The load from Jack 3 simulated the concentrated load from the upper column foot, and it was monitored with a 500 kN load cell. Five 360 mm long, 20 mm thick steel plates were placed at each loading point to distribute the load on the timber beams, and they also served as the floor slab to limit the out-of-plane deformation of beams. The arrangement of measuring points is shown in Figure 9c. Six 100mm linear variable displacement transducers (LVDTs) were used to measure the displacement. Two of them were installed on each side of the load cell below jack 3 and on top of the tenon joint formed by the beam ends to measure the vertical displacement. Four LVDTs were used to monitor the vertical displacements at mid-span of each beam and at each end of the Dianmu. A total of 62 electrical resistance strain gauges were utilized for the strain measurement at selected points of the components. More details are referred to Yang and Qin (2018).

The floor load on top of the beams was constant throughout the experiment, whereas the load carried by the upper column can be varied. The loading procedure consisted of two sequential steps:

(1) Load (F_{UL}) was applied via Jacks 1 and 2 simultaneously at 2.5 kN increments (each jack) until F_{UL} reached 80 kN which is the estimated equivalent floor load from site.

(2) Load (F_{CL}) was applied by Jack 3 at 5 kN increments until the specimen failed.

The loading procedure was in accordance with the Standard for test method of timber structures (MOHURD 2012).

Experimental Results

Figure 10 shows the load-displacement curves of the five specimens. The load F_{tot} is the vertical load truly carried by the Tibetan BCJ, as determined by Eq. (4). The load increased linearly with displacement in the initial stage. The relationship between load and displacement became nonlinear after yielding of timber at the bottom of Dianmu (for example, when the load reached F_{tot} =108.11 kN for the BCJ specimen with Queti-inclination angle $\theta = 9°$, the collected strain at #S40 at the bottom of Dianmu was 11278 $\mu\varepsilon$ exceeding the yield strain 10329 $\mu\varepsilon$). It was noted from Table 4 that the load-carrying capacity of the joint decreased with increasing Queti-inclination angle.

Substituting the parameters of the specimens in Tables 1 and 2 into Eqs. (5), (6), (15), (19), (26) and (31), the yield and ultimate loads of the joint with different Queti-inclination angles are calculated respectively. These predicted values of load-carrying capacity are then compared with the experimental values in Table 5. It is noted that

(1) For joint without Queti-inclination, the predicted yield load F_y and ultimate load F_u, are 2.4% and 1.6% respectively lower than the test results. They are noted in close agreement.

(2) For joints with Queti-inclination, the predicted yield load agrees well with the test values with a maximum error of 3.8% only. The predicted ultimate load is also close to the test value when the Que-inclination angle is small at 3° and 6°. The error is larger at 13.2% when the angle is 12° with conservative prediction.

The errors observed in the above comparison may be due to the followings:

(1) Timber is a kind of naturally biological material with large variability in the mechanical properties which may lead to uncertainty in the structural model of the joint.

(2) The reduction coefficients of the effect of size and defects on timber strength are obtained from the handbook (Long 2005). These values are determined from statistical results.

(3) There are errors in the laboratory tests including those in preparing the timber components, assembly of the joint, as well as in the loading process.

The above comparison shows that the predicted values and test results of the yield and ultimate loads are close to each other. It may therefore be conservative but safe to use the proposed analytical model for evaluating the load-carrying capacity of the joint with Queti-inclination.

Parametric Studies

The effects of material property, Queti width and height, as well as the dowel height on the load-carrying capacity of the Tibetan BCJ under vertical load are studied with the proposed model.

Mechanical Properties of Timber

The estimation of load-carrying capacity of a BCJ in an existing structure is usually conducted via full-scale model test on specimens prepared from new timber. How the effects of different mechanical properties of timber can be considered in the evaluation is vital to the accuracy of prediction.

Table 6 shows the mechanical properties of old timber coming from the structural components of a heritage Tibetan building. Table 2 shows those of new timber from Mongolian Scotch pine (*Pinus sylvestris var. mongolica Litv.*). The mechanical properties of the old timber are poorer compared with the new timber. The load-carrying capacities of the joints with new and old timber are obtained by substituting the values of mechanical properties in Tables 2 and 5 into the analytical model, and they are shown in Figure 11a. It is observed that the changes of yield and ultimate loads of BCJs with Queti-inclination angle are similar for the new and old timber, but the load-carrying capacity of the joint from old timber is obviously lower than that from new timber with the largest reductions of 87 kN in F_y and 111 kN in F_u.

Queti Width

The width of Dianmu is slightly larger than that of Gongmu in a Tibetan BCJ with the ratio w_d/w_g ranging from 1.1 to 1.2 in general (Ngawang 2007). In this section, the effect of Queti width on the load-carrying capacity of the joint is analyzed by varying the widths of Dianmu and Gongmu but with the same w_d/w_g proportion. When the widths of Dianmu and Gongmu take up values of ($w_d = 150\text{mm}$, $w_g = 127\text{mm}$), ($w_d = 165\text{mm}$, $w_g = 140\text{mm}$) and ($w_d = 180\text{mm}$, $w_g = 153\text{mm}$), the variation of yield and ultimate loads of the joints with Que-inclination is shown in Figure 11b. It is noted that:

(1) For the BCJs with the same Queti-inclination angle, F_y and F_u increase with the Queti width with the largest increments of 25 kN in F_y and 47 kN in F_u.

(2) The critical thresholds θ_{cr} corresponding to R-failure of the joints are 31.4°, 32.7° and 34.1° for $w_d = 150\text{mm}$, 165mm and 180mm, respectively, indicating θ_{cr} increases with the Queti width with the largest increment of 2.7°.

Queti Height

The heights of Dianmu and Gongmu, i.e. h_d and h_g, are varied with the same h_d/h_g proportion to study the effect of Queti height ($h_Q = h_d + h_g$) on the load-carrying capacity of the joint. The variation of yield and ultimate loads with Que-inclination angle for $h_Q = 250$mm ($h_d =$ 86 mm, $h_g = 164$ mm), $h_Q = 290$ mm ($h_d = 100$ mm, $h_g = 190$ mm) and $h_Q = 330$ mm ($h_d = 114$mm, $h_g = 216$mm) are shown in Figure 11c. It is noted that:

(1) The variation of Queti height has no effect on the load-carrying capacity of the joint without Queti-inclination.

(2) For the joints with the same Queti-inclination angle, F_y and F_u decrease with the Queti height with the largest reductions of 5 kN in F_y and 58 kN in F_u. This is because the additional bending moment induced by the same Queti-inclination angle increases with the Queti height.

(3) The critical thresholds θ_{cr} corresponding to R-failure of the joints are 36.7°, 32.7° and 29.4° for $h_Q = 250$mm, 290mm and 330mm, respectively, indicating θ_{cr} is reduced with the Queti height with the largest reduction of 7.3°, which is opposite to the effect of Queti width.

Dowel Height

The relationships between the load-carrying capacity of the joint and the Queti-inclination angle for dowel height h_a = 150mm, 100mm and 50mm are shown in Figure 11d. It is noted that:

(1) When $\theta < \theta_{dg'} = 24°$, the load-bearing surface of Dianmu is in full compression, and the dowel height has no effect on the load-carrying capacity of the joint.

(2) When $\theta \geq \theta_{dg'} = 24°$, the critical thresholds θ_{cr} corresponding to R-failure of the joints are 39.1°, 32.7° and 27.8° for h_a=150mm, 100mm and 50mm, respectively, indicating θ_{cr} decreases with the dowel height with the largest reduction of 11.3°. A

smaller dowel height also leads to a sharper reduction of ultimate load with the Queti-inclination angle.

(3) The dowels of Tibetan BCJs may experience shrinkage and decay during the hundreds of years of service. This will reduce the load-carrying capacity of the joint when the angle of Queti-inclination exceeds the threshold angle corresponding to the critical state of full compression. However, since the dowel is hidden inside the mortise (Figure 1c), its effective size at current state cannot be directly obtained, and some devices, such as the radar scanner or damage detector, are needed to determine the dowel height for an accurate evaluation of its contribution to the load-carrying capacity of the joints in Tibetan heritage buildings.

Conclusions

An analytical model of Tibetan BCJ with Queti-inclination is proposed for evaluating the load-carrying capacity of the joint under vertical load. Experimental results show that the proposed model is effective and reliable to predict the yield load and ultimate load of the Tibetan BCJ. The following conclusions may be drawn from this study.

(1) Dianmu is the most important and yet the weakest component of the Tibetan BCJ to resist the vertical load. The joint fails due to the UC-failure when Queti is upright, and it fails due to the EC-failure when the Queti-inclination angle is smaller than the critical threshold θ_{cr}. The failure mode may change into R-failure when the inclination angle reaches θ_{cr}. Generally, the joint will not fail in the S-failure mode.

(2) The load-carrying capacity of the joint with Queti-inclination is related not only to the inclination angle, but also to the dimensions of its component.

(3) Parametric studies with the proposed model show the following observations. (i) Poor mechanical properties of old timber in the structure may reduce significantly the load-carrying capacity of the joint with the largest reductions of 87 kN in F_y and 111 kN in

F_u. (ii) The Queti width and height have an opposite effect on the structural performances of the joint. The yield and ultimate loads and the critical threshold angle increase with the Queti width with the largest increments of 25 kN in F_y, 47 kN in F_u and 2.7° in θ_{cr}, while they decrease with the Queti height with the largest reductions of 5 kN in F_y, 58 kN in F_u and 7.3° in θ_{cr}. (iii) The dowel height has no effect on the load-carrying capacity of the joint when θ is smaller than 24°, i.e. the angle θ_{dg}, corresponding to the critical state of full compression at the load-bearing surface of Dianmu. When θ is greater than 24°, the critical threshold angle θ_{cr} decreases with the dowel height with the largest reduction of 11.3° and a smaller height of dowel will lead to a sharper reduction of ultimate load with the Queti-inclination angle.

The load-carrying capacity estimated by the analytical model proposed in this paper can provide useful reference for the decisions on issues such as "how many tourists (a kind of vertical load) can be sustained" and "whether the maintenance is needed" of Tibetan heritage timber buildings.

Disclosure statement

No potential conflict of interest was reported by the authors.

Acknowledgments

The work described in this paper was financially supported by the Hainan Provincial Natural Science Foundation of China (520QN230), Beijing Natural Science Foundation of China (8151003), National Key Research and Development Project (2019YFD1101003), National Natural Science Foundation of China (51778045, 52068019), the 111 Project of China (B13002) and Science Foundation of Hainan University [KYQD(ZR)1975]. The comments from Prof. S.S. Law and his help in polishing the English usage of this paper are also acknowledged.

References

Cao, J. X., Zhao, Y., Liu Y. Y., Lu H. Y., and Wang W. H. 2021. Load-carrying capacity analysis of traditional Chinese Dou-gong joints under monotonic vertical and reversal lateral loading. *J. Build. Eng.* 44(2):102847. doi: 10.1016/j.jobe.2021.102847.

Chang, W. S., and Hsu, M. F. 2007. Rotational performance of traditional Nuki joints with gap II: The behavior of butted Nuki joint and its comparison with continuous Nuki joint. *J. Wood Sci.,* 53(5):401–407. doi: 10.1007/s10086-007-0880-1.

Chen, C. C., Qiu, H. X., and Lu, Y. 2016a. Flexural behavior of timber dovetail mortise-tenon joints. *Constr. Build. Mater.,* 112:366-377.

Chen, Z. Y., Zhu, E. C., Lam, F., and Pan, J. 2014. Structural performance of Dou-Gong brackets of Yingxian Wooden Pagoda under vertical load – An experimental study. *Eng. Struct.,* 80:274-288. doi: 10.1016/j.engstruct.2014.09.013.

Chen, Z. Y., Zhu, E. C., Pan, J. L., and Wu, G. F. 2016b. Energy-dissipation performance of typical beam-column joints in Yingxian Wood Pagoda: experimental study. *J. Perform. Constr. Facil.,* 30(3): 04015028. doi: 10.1061/(ASCE)CF.1943-5509.0000771.

Chun Q., Jin H., Dong Y. H., Hua Y. W., and Han Y. D. 2020. Research on mechanical properties of Dingtougong mortise-tenon joints of Chinese traditional Hall-style timber buildings built in the Song and Yuan Dynasties. *Int. J. Archit. Herit.* 14(5):729-750. doi: 10.1080/15583058.2019.1568613.

He J. X., Wang J., and Yang Q. S. 2017. Theoretical and experimental analysis on mechanical behavior of column in traditional timber structure during rocking. *J. Build. Struct.,* 34(11):50-58. doi: 10.6052/j.issn.1000-4750.2016.07.0527.

Jiang, H. Y. 1994. *The maintenance report of Potala Palace.* Cultural Relics, Beijing.

Li, P., Yang, N., and Wang, Y. 2013. Research on structural present state and damage reasons of ancient Tibetan buildings. *Appl. Mech. Mater.,* 351-352, 1652-1656.

Li S. C., Chen L. K., Jiang L. Z., and Li J. Q. 2020. Experimental investigation on the seismic behavior of the semi-rigid one-way straight mortise-tenon joint of a historical timber building. *Int. J. Archit. Herit.* 14(8):1135-1147. doi: 10.1080/15583058.2019.1587041.

Liu, H. W. 2011. *Mechanics of materials,* Higher Education Press, Beijing.

Long, W. G. 2005. *Handbook of timber structure design,* China Architecture and Building Press, Beijing.

Lyu, M. N., Zhu, X. Q., and Yang, Q. S. 2017. Connection stiffness identification of historic timber buildings using Temperature-based sensitivity analysis. *Eng. Struct.,* 131, 180-191. doi: 10.1016/j.engstruct.2016.11.012.

MOHURD (Ministry of Housing, and Urban-Rural Development of the People's Republic of China). 2012. *Standard for test methods of timber structures GB/T50329-2012*, China Architecture and Building, Beijing.

Ngawang, R. 2007. *Tibetan architecture overview,* Sichuan Fine Arts, Chengdu.

Ogawa K., Sasaki Y., and Yamasaki M. 2015. Theoretical modelling and experimental study of Japanese "Watari-ago" joints. *J. Wood Sci.,* 61:481–491. doi: 10.1007/s10086-015-1509-4.

Pan, Y., Wang, C., Tang, L. N., and Li, L. J. 2015. Study on mechanical model of straight-tenon joints in ancient timber structures. *Eng. Mech.,* 32(2):82-89. doi: 10.6052/j.issn.1000-4750.2013.08.0728.

Qin, S. J., and Yang, N. 2017. Effect of queti-inclination on mechanical properties of typical Tibetan timber beam-column joint. *Proc., 4th Int. Conf. on Structural Health Assessment of Timber Structures,* Istanbul, Turkey, 463-471.

Qin, S. J., and Yang, N. 2018. Strength degradation and service life prediction of timber in ancient Tibetan building. *Eur. J. Wood Wood Prod.,* 76(2): 731-747. doi: 10.1007/s00107-017-1211-x.

SAC (Standardization Administration of China). 2009. Testing methods for physical and mechanical properties of wood. *GB/T 1928-2009,* Beijing.

SWRACW (Subcommittee on Wood Research of the ASCE Committee on Wood). 1986. Structural wood research needs. *J. Struct. Eng.,* 112(9): 2155-2165.

Wang, J, He, J. X. Yang, Q. S., and Yang, N. 2018. Study on mechanical behaviors of column foot joint in traditional timber structure. *Struct. Eng. Mech.,* 66(1):1-14. doi: 10.12989/sem.2018.66.1.001.

Xie, Q. F., Du, B., Zhang, F. L., Zheng, J. P., and Xu, Q. F. 2014. Theoretical analysis on moment-rotation relationship of dovetail joints for Chinese ancient timber structure buildings. *Eng. Mech.,* 31(12):140-146. doi: 10.6052/j.issn.1000-4750.2013.08.0751.

Xie Q., Wang L., Zhang L., Xiang W., and Hu W. 2020. Rotational behaviors of fork-column Dou-Gong: experimental tests and hysteresis model. *J. Perform. Constr. Facil.,* 34(3):04020032. doi: 10.1061/(ASCE)CF.1943-5509.0001426

Yan, H. C. 2011. The experimental and finite element analysis of Tibetan wooden frame system. M.S. thesis, Beijing Jiaotong Univ., Beijing, China.

Yang, N., Li, P., Law, S. S., and Yang, Q. S. 2012. Experimental research on mechanical properties of timber in ancient Tibetan building. *J. Mater. Civ. Eng.,* 24:635-643. doi: 10.1061/(ASCE)MT.1943-5533.0000438.

Yang, N., and Qin, S. J. 2018. Effect of queti-inclination angles on structural performance of Tibetan timber beam-column joints. *J. Perform. Constr. Facil.,* 32(3): 04018013. doi: 10.1061/(ASCE)CF.1943-5509.0001156.

Yang, N., and Yan, H. C. 2012. Transfer mechanism analysis of typical beam-column connection in ancient Tibetan architecture. *J. Beijing Jiaotong Univ.,* 36(4):76-81. doi: 10.3969/j.issn.1673-0291.2012.04.015.

Zhu, L. 2016. Study on the seismic performance of ancient Tibetan timber structure. M.S. thesis, Beijing Jiaotong Univ., Beijing, China.

Figures

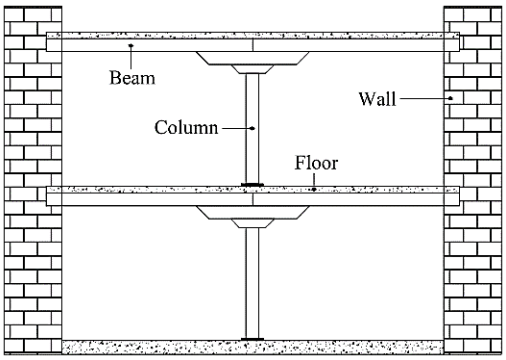

(a) supporting system in typical Tibetan structure

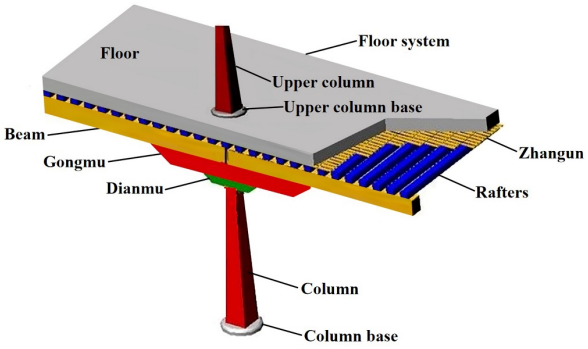

(b) composition and arrangement of typical Tibetan floor

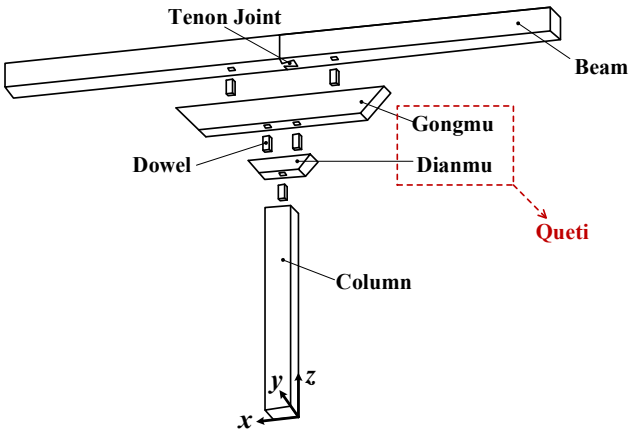

(c) construction of Typical Tibetan timber BCJ

Figure 1. Typical Tibetan structure and beam-column joint

Figure 2. Queti-inclination in practice

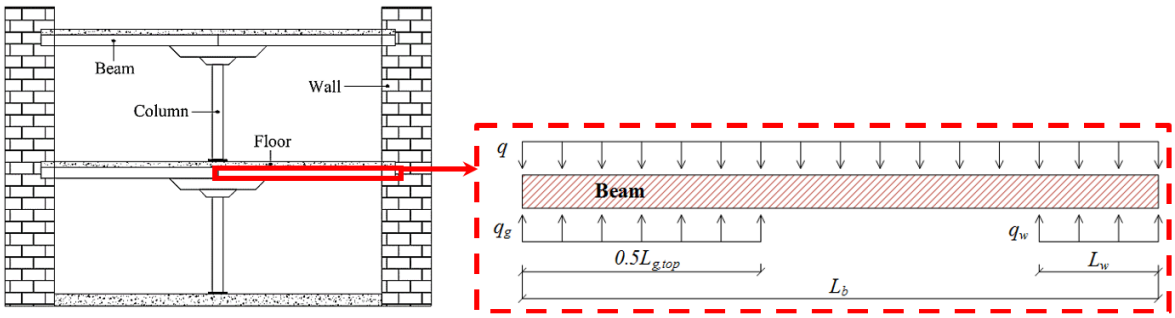

Figure 3. Force diagram of beam under uniform load

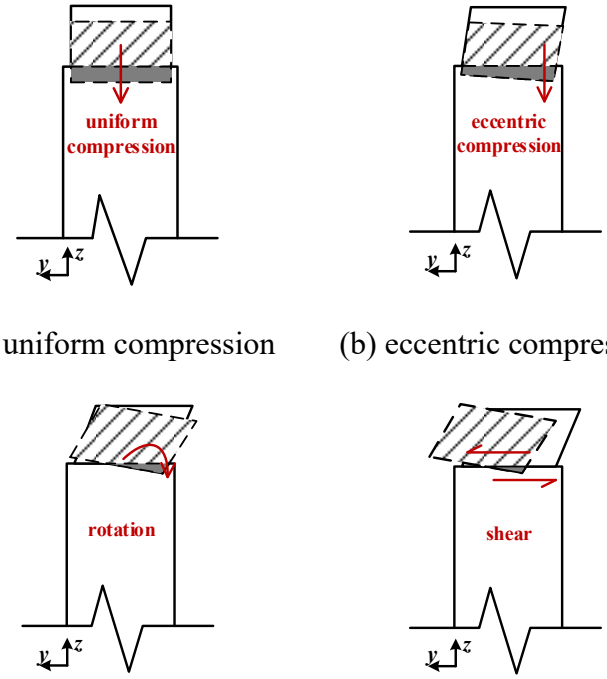

(a) uniform compression (b) eccentric compression

(c) rotation deformation (d) shear deformation

Figure 4. Failure modes of the joint

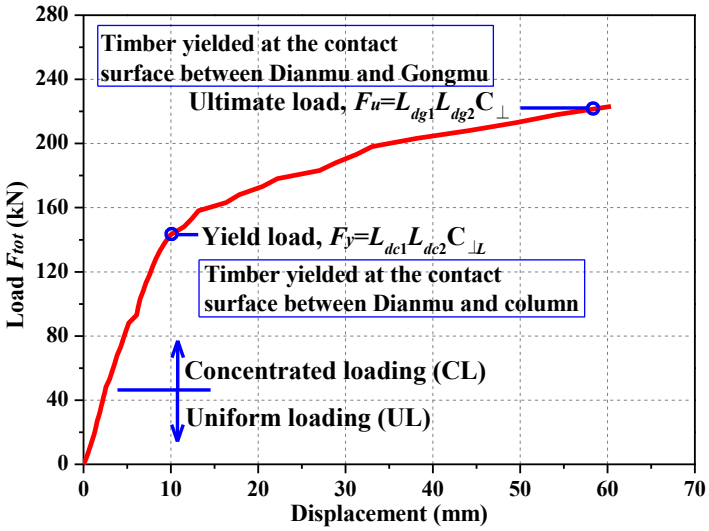

Figure 5. Experimental load-displacement curve of the joint without Queti-inclination

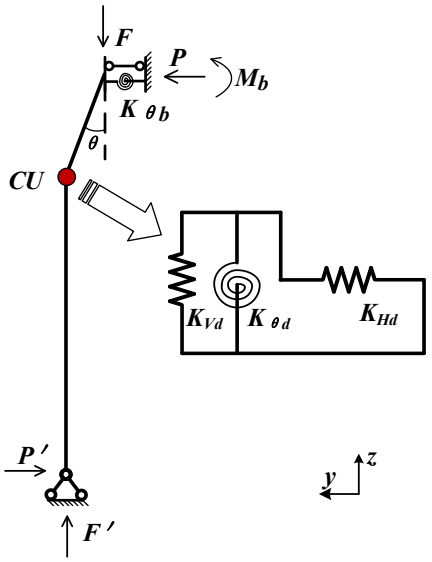

Figure 6. Simplified analytical model of Tibetan BCJ with Queti-inclination

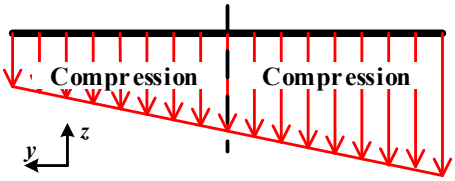

(a) full compression

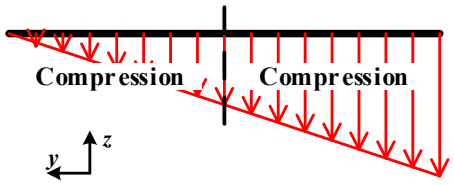

(b) critical state

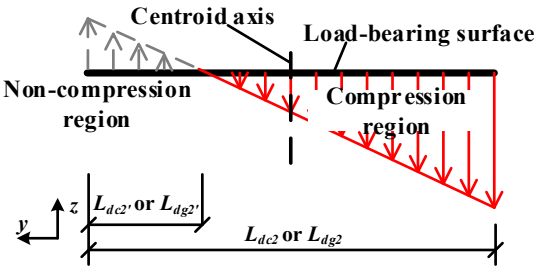

(c) partial compression

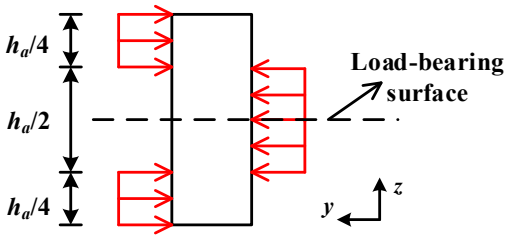

(d) horizontal stress state of the dowel

Figure 7. Change of stress distribution on load-bearing surface of Dianmu with increasing Queti-inclination angle

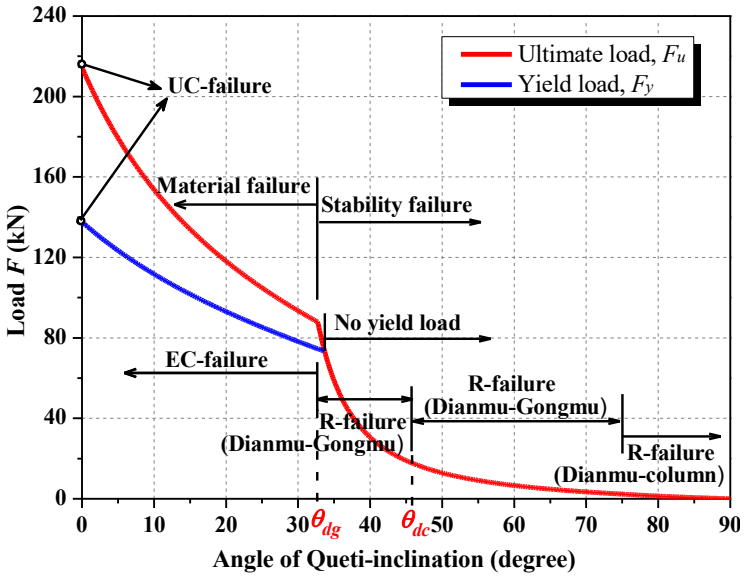

Figure 8. Typical variation of load-carrying capacity with angle of Queti-inclination

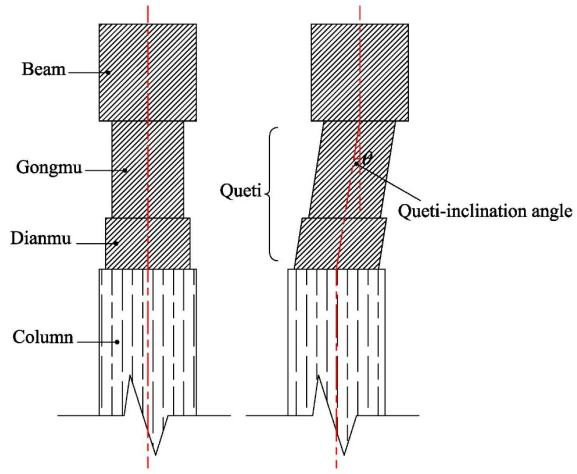

(a) BCJ specimens with Queti-inclination

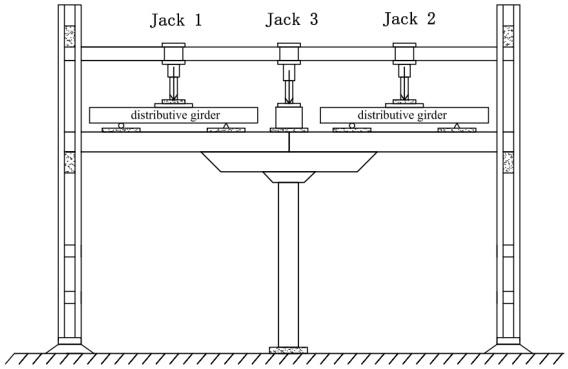

(b) loading equipment

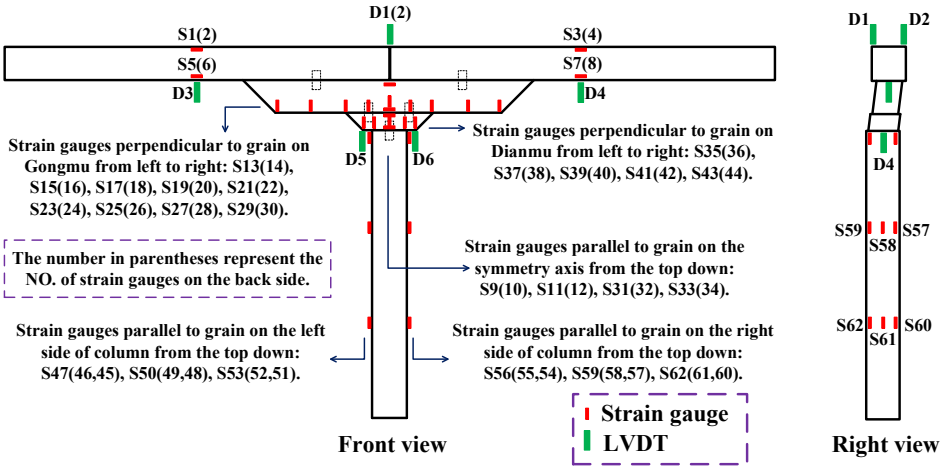

(c) arrangement of measuring points

Figure 9. Schematic diagram of test specimens and loading equipment

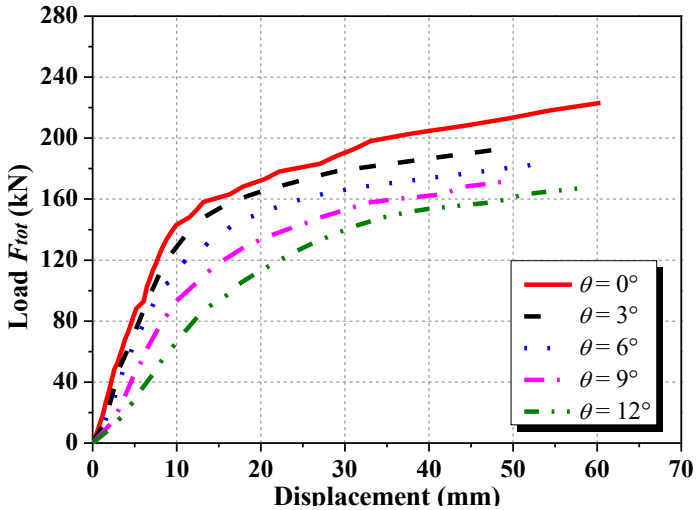

Figure 10. Experimental load-displacement curves of BCJ specimens with different Queti-inclination angles

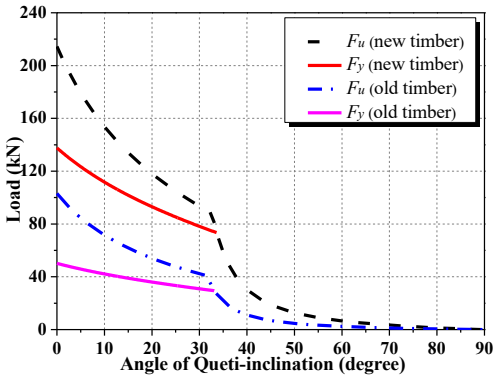

(a) effect of material properties

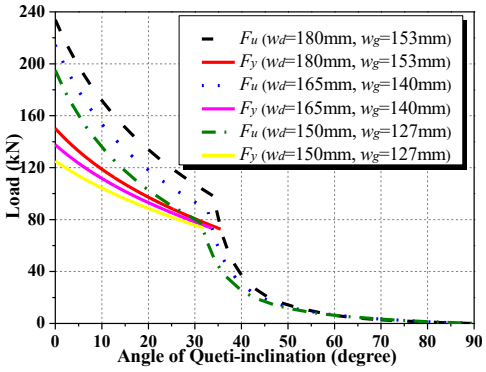

(b) effect of Queti width

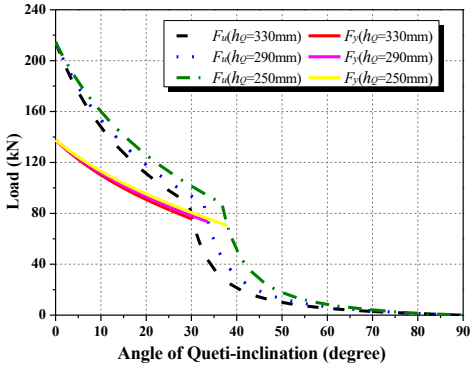

(c) effect of Queti height

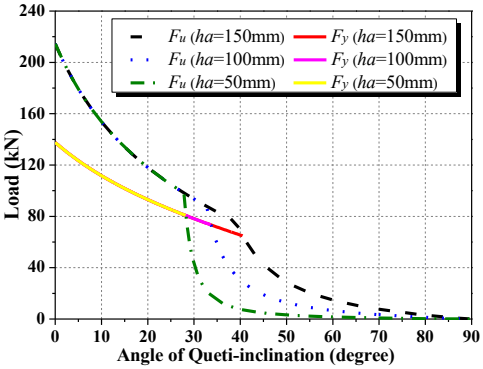

(d) effect of dowel height

Figure 11. Effects of material and size of components on load-carrying capacity

Tabless

Table 1. Dimensions of Components (mm)

Components	Bottom surface (Length×Width)	Top surface (Length×Width)	Height
Beam	2200×190	2200×190	190
Gongmu	1300×140	1680×140	190
Dianmu	300×165	500×165	100
Column	190×190	190×190	1630
Dowel	40×40	40×40	100

Table 2. Mechanical Properties of New Timber Used in Laboratory Tests (MPa)

$E_{\perp}$	$G_{\parallel}$	$C_{\perp}$	$C_{\perp L}$
425	351	2.60	4.39

Note: $E_{\perp}$ denotes the modulus of elasticity perpendicular to grain; $G_{\parallel}$ denotes the shear modulus parallel to grain; $C_{\perp}$ denotes the yield strength under all-area compression perpendicular to grain; $C_{\perp L}$ denotes the yield strength under partial-area compression perpendicular to grain.

Table 3. Adjustment Coefficients of Mechanical Properties of Timber Component

Mechanical indexes	α	K_{Q1}	K_{Q2}	K_{Q3}	K_{Q4}
$E_{\perp}$	0.055	0.75	0.66	0.90	1.00
$G_{\parallel}$	0.012	0.90	0.70	0.82	1.00
$C_{\perp}$	0.045	0.75	0.66	0.90	1.00
$C_{\perp L}$	0.045	0.75	0.66	0.90	1.00

Table 4. Performance Parameters of BCJs in Laboratory Tests (kN)

θ (degree)	F_y	F_u
0	140.96	218.00
3	133.88	194.82
6	122.44	182.38
9	110.18	174.00
12	106.35	167.44

Table 5. Comparison of Predicted Values with Tested Results (kN)

θ (degree)	F_y			F_u		
	Prediction	Test	Error	Prediction	Test	Error
0	137.63	140.96	-2.4%	214.50	218.00	-1.6%
3	128.75	133.88	-3.8%	191.96	194.82	-1.5%
6	120.92	122.44	-1.2%	173.61	182.38	-4.8%
9	113.91	110.18	3.4%	158.31	174.00	-9.0%
12	107.56	106.35	1.1%	145.30	167.44	-13.2%

Note: error $=$ (prediction $-$ test)/test $\times$ 100%.

Table 6. Mechanical Properties of Old Timber Used in Heritage Building (MPa)

$E_{\perp}$	$G_{\parallel}$	$C_{\perp}$	$C_{\perp L}$
237	247	1.25	1.60